REVIEW SUMMARY

MATERIALS SCIENCE

Building devices from colloidal quantum dots

Cherie R. Kagan,* Efrat Lifshitz,* Edward H. Sargent,* Dmitri V. Talapin*

BACKGROUND: The Information Age was founded on the semiconductor revolution, marked by the growth of high-purity semiconductor single crystals. The resultant design and fabrication of electronic devices exploit our ability to control the concentration, motion, and dynamics of charge carriers in the bulk semiconductor solid state.

Our desire to introduce electronics everywhere is fueled by opportunities to create intelligent and enabling devices for the information, communication, consumer product, health, and energy sectors. This demand for ubiquitous electronics is spurring the design of materials that exhibit engineered physical properties and that can enable new fabrication methods for low-cost, large-area, and flexible devices.

Semiconductors, which are at the heart of electronics and optoelectronics, come with high demands on chemical purity and structural perfection. Alternatives to silicon technology are expected to combine the electronic and optical properties of inorganic semiconductors (high charge carrier mobility, precise n- and p-type doping, and the ability to engineer the band gap energy) with the benefits of additive device manufacturing: low cost, large area, and the use of solution-based fabrication techniques. Along these lines, colloidal semiconductor quantum dots (QDs), which are nanoscale crystals of analogous bulk semiconductor crystals, offer a powerful platform for device engineers. Colloidal QDs may be tailored in size, shape, and composition and their surfaces functionalized with molecular ligands of diverse chemistry. At the nanoscale (typically 2 to 20 nm), quantum and dielectric confinement effects give rise to the prized size-, shape-, and composition-tunable electronic and optical properties of QDs. Surface ligands enable the stabilization of QDs in the form of colloids, allowing their bottom-up assembly into QD solids. The physical properties of QD solids can be designed by selecting the characteristics of the individual QD building blocks and by controlling the electronic communication between the QDs in the solid state. These QD solids can be engineered with application-specific electronic and optoelectronic properties for the large-area, solution-based assembly of devices.

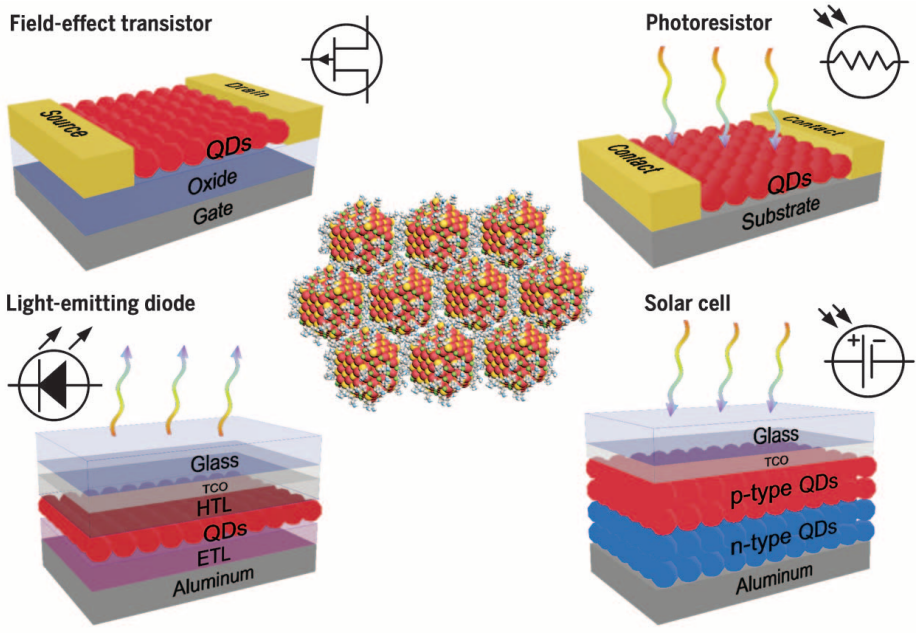

Colloidal quantum dot device architectures. Colloidal quantum dots (center) may be engineered in size, shape, and surface chemistry and deposited from solution to be integrated as thin-film solids in different electronic and optoelectronic devices that modulate and transmit charge and transduce light and electricity. [Figure courtesy of O. Voznyy and F. S. Stinner]

ADVANCES: The large surface-to-volume ratio of QDs places a substantial importance on the composition and structure of the surface in defining the physical properties that govern the concentration, motion, and dynamics of excitations and charge carriers in QD solids. Recent studies have shown pathways to passivate uncoordinated atoms at the QD surface that act to trap and scatter charge carriers. Surface atoms, ligands, and ions can serve as dopants to control the electron affinity of QD solids. Surface ligands and surrounding matrices control the barriers to electronic, excitonic, and thermal transport between QDs and between QDs and matrices. New ligand chemistries and matrix materials have been reported that provide freedom to control the dynamics of excitons and charge carriers and to design device interfaces. These advances in engineering the chemical and physical properties of the QD surface have been translated into recent achievements of high-mobility transistors and circuits, high-quantum-yield photodetectors and light-emitting devices, and high-efficiency photovoltaic devices.

ON OUR WEBSITE

Read the full article at http://dx.doi.org/10.1126/science.aac5523

OUTLOOK: The dominant role and dynamic nature of the QD surface, and the strong motive to build novel QD devices, will drive the exploration of new surface chemistries and matrix materials, processes for their assembly and integration with other materials in devices, and measurements and simulations with which to map the relationship between surface chemistry and materials and device properties. Challenges remain to achieve full control over the carrier type, concentration, and mobility in the QD channel and the barriers and traps at device interfaces that limit the gain and speed of QD electronics. Surface chemistries that allow for both long carrier lifetime and high carrier mobility and the freedom to engineer the bandgap and band alignment of QDs and other device layers are needed to exploit physics particular to QDs and to advance device architectures that contribute to improving the performance of QD optoelectronics. The importance of thermal transport in QD solids and their devices is an essential emerging topic that promises to become of greater importance as we develop QD devices.

The list of author affiliations is available in the full article online.
*Corresponding author. Email: kagan@seas.upenn.edu (C.R.K.); ssefrat@technion.ac.il (E.L.); ted.sargent@utoronto.ca (E.H.S.); dvtalapin@uchicago.edu (D.V.T.)
Cite this article as C. R. Kagan *et al.*, *Science* 353, aac5523 (2016). DOI: 10.1126/science.aac5523

REVIEW

MATERIALS SCIENCE

Building devices from colloidal quantum dots

Cherie R. Kagan,[1]* Efrat Lifshitz,[2]* Edward H. Sargent,[3]* Dmitri V. Talapin[4,5]*

The continued growth of mobile and interactive computing requires devices manufactured with low-cost processes, compatible with large-area and flexible form factors, and with additional functionality. We review recent advances in the design of electronic and optoelectronic devices that use colloidal semiconductor quantum dots (QDs). The properties of materials assembled of QDs may be tailored not only by the atomic composition but also by the size, shape, and surface functionalization of the individual QDs and by the communication among these QDs. The chemical and physical properties of QD surfaces and the interfaces in QD devices are of particular importance, and these enable the solution-based fabrication of low-cost, large-area, flexible, and functional devices. We discuss challenges that must be addressed in the move to solution-processed functional optoelectronic nanomaterials.

The development of modern electronics in the middle of the 20th century has changed the course of human society. Semiconductor crystals, typically of silicon, are used to build high-performance electronic circuits, solar cells, and light detectors. Today, electronics have become increasingly pervasive, and semiconductor devices are fabricated from a broader range of materials and introduced in more diverse forms, from microscopic sensors and implants to mobile devices to TVs, whose active components span meters in size. Solar farms use square miles of semiconductor panels to generate electricity at grid parity cost.

However, semiconductor fabrication processes, originally developed for small chips, become costly when applied to devices with a large form factor. Conventional semiconductor devices are also characteristically planar and rigid. In constrast, emerging applications often require ultracheap electronic devices and their integration on flexible and curved surfaces such as paper, fabric, and plastic.

In recent years, the "one crystal per device" concept has been challenged by the development of materials and processes that allow bottom-up fabrication, in which device parts are assembled from nanoscale components—such as semiconductor quantum dots (QDs), carbon nanotubes, and polymers—by using nontraditional techniques, such as solution-based and additive manufacturing. However, the shift from materials that are bulk single crystals to assemblies of many components introduces challenges, most notably the increased role of interfaces. Interfaces often introduce bottlenecks to charge transport and can also function as recombination sites that reduce carrier lifetime, leading to lower device performance.

Colloidal semiconductor QDs open up opportunities to integrate inorganic semiconductors, with a proven track record in electronic and optoelectronic devices, into high-performance and flexible devices by using low-temperature, large-area, solution-based methods instead of by costly, high-vacuum, high-temperature device manufacturing processes. Tuning of QD size, shape, or building heterostructures into each QD introduces tools for engineering electronic materials with properties not available in traditional bulk semiconductors.

From bulk crystals to QD arrays

Colloidal QDs are a subset of semiconductor nanocrystals (NCs), which at typical 2- to 20-nm diameters show effects of quantum confinement. Each QD contains hundreds to thousands of atoms (Fig. 1A). These colloidal QDs are commonly made of II-VI, III-V, and IV-VI semiconductors by means of inexpensive and scalable, wet-chemical synthetic procedures (*1*, *2*). The synthetic methodology for a wide range of technologically important semiconductors has been advanced to provide QD samples tunable in size and shape and with near-atomic-layer precision (*1*). The surface of as-synthesized QDs is coated with a layer of molecular ligands (Fig. 1A). These ligands stabilize colloidal QDs against precipitation (Fig. 1B), enabling QD inks that can be processed into thin-film electronic and optoelectronic devices through coating and printing techniques (*3*).

After evaporation of the carrier solvent, arrays of QDs form a solid material whose structure depends most notably on the size and shape uniformity of the individual QDs and the solvent characteristics and evaporation rate. A large dispersity in QD size or shape and a fast solvent evaporation rate tend to pack QDs in glassy solids with only short-range order (Fig. 1C, bottom). On the other hand, slow evaporation of the carrier solvent from a colloidal dispersion of QDs with tight size and shape distribution often leads to the formation of long-range ordered superlattices or supercrystals (Fig. 1C, top) (*1*). Either glassy or ordered QD arrays may also be assembled from two different types of QDs in order to form multicomponent QD arrays (*4*, *5*). Such superlattices should be considered supramolecular analogs of atomic crystals, whereas glassy QD films are the cousin of amorphous solids. These QD solids, ordered or amorphous, are used as active components of electronic and optoelectronic devices (*2*). A device can contain one or several QD layers, resembling a multilayer stack of active components in traditional semiconductor devices. Although this Review focuses on semiconductor QDs, colloidal NCs of various materials—including metal oxides, metals, dielectrics, and magnets—can be used in the solution-based fabrication of device components (*6*). The chemistry of surface ligands dictates the dispersability of QDs in different solvents, a topic that is particularly important for the fabrication of multilayered structures that require the deposition of QD colloids from mutually orthogonal solvents (such as polar dimethylformamide and nonpolar hexane).

The core and the surface of individual QDs

The electronic structure of semiconductor QDs differs fundamentally from that of the corresponding bulk material as a result of quantum and dielectric confinement effects. In bulk semiconductors, the large density (~10^{22} cm^{-3}) of covalently and/or ionically bonded atoms creates a high and broad density of conduction and valence band states. The conduction and valence bands are energetically separated by the band gap, which is empty of states (Fig. 2A). Instead of continuous valence and conduction bands, QDs develop discrete states whose energy and symmetry depend on QD size and shape (Fig. 2A). The energy gaps between the states decrease with increasing QD size, thus relating the energy gap between the highest occupied and lowest unoccupied states to the QD size (*7*, *8*).

The large surface-to-volume ratio of QDs introduces a substantial importance on the nature of the surface. A QD surface exposes different crystal facets and creates dangling bonds. Undercoordinated surface atoms often contribute electronic states with energies lying within the band gap of the QD core (Fig. 2B). These surface states alter the electronic and optical properties of QDs because low-energy states may serve as dopants, and deeper band-tail and mid-gap states may act

[1]Department of Electrical and Systems Engineering, Department of Materials Science and Engineering, and Department of Chemistry, University of Pennsylvania, 200 South 33rd Street, Philadelphia, PA 19104, USA. [2]Schulich Faculty of Chemistry, Solid State Institute and Russell Berrie Nanotechnology Institute, Technion, Haifa 32000, Israel. [3]Department of Electrical and Computer Engineering, 10 King's College Rd, Toronto ON M5S 3G4, Canada. [4]Department of Chemistry and James Franck Institute, University of Chicago, Chicago, IL 60637, USA. [5]Center for Nanoscale Materials, Argonne National Laboratory, Argonne, IL 60439, USA.
*Corresponding author. Email: kagan@seas.upenn.edu (C.R.K.); ssefrat@technion.ac.il (E.L.); ted.sargent@utoronto.ca (E.H.S.); dvtalapin@uchicago.edu (D.V.T.)

to trap charge carriers and provide a path for fast electron-hole recombination (*9*).

Dangling bonds can be satisfied by engaging surface atoms in strong chemical bonding with ligands. This pushes the energy of the occupied surface states below and the unoccupied surface states above the corresponding states of the QD core (Fig. 2C). For example, modifying the surface ligand chemistry for PbS QDs has been used to passivate electronic states, increasing the QD photoluminescence efficiency and the power conversion efficiency of QD solar cells (*10*, *11*).

The understanding of QD surfaces has dramatically improved in recent years (*12*). The combination of electronic, optical, and vibrational spectroscopies (*13*–*16*), nuclear magnetic resonance (*15*, *17*), x-ray and ultraviolet photoelectron spectroscopy (*18*), and high-resolution electron microscopy (*19*) has been used to reveal the arrangement of surface atoms in the QD core, the density and packing of the ligand molecules in the corona surrounding the QD core, and the influence of ligands on the QD electronic structure (*20*, *21*). The integration of experimental techniques and computational methods such as density functional theory and molecular dynamics provides complementary information on the interactions that govern surface structure and binding and enable the construction of compelling models of the QD-ligand interface (*22*, *23*).

The interactions between the QD core and ligand head-group can be rationalized by using the concepts originally developed for molecular coordination compounds and recently adapted to NC surfaces (*24*, *25*). Generally, electron-deficient metal ions at the QD surface interact with electron-rich nucleophilic ligands. These ligands can be either neutral molecules with lone electron pairs such as amines (RNH_2) and phosphines (R_3P) or ionic species such as carboxylate ($RCOO^-$) and various inorganic ions (for example, Cl^-, SnS_4^{4-}). The surface of metal chalcogenides and other compound QDs also exposes electron-rich sites that can interact with electrophilic species, such as $Cd(OOCR)_2$ or $PbCl_2$, that bind to the QD surface via empty orbitals on metal atoms (*25*). These bonding motifs are schematically shown in Fig. 2D. The requirement for QD charge neutrality as a whole constrains the composition of the inorganic core, depending on the type of surface ligands. The QD core can be either stoichiometric, if all ligands are neutral species, or deviate from the stoichiometry of the corresponding parent material, when ligands are charged. CdSe and PbSe QDs synthesized in the presence of carboxylate ligands show metal-to-selenium ratios significantly in excess of unity (*26*, *27*). Binding of small ions, such as OH^- and Cl^-, helps to match the density of ligand coating to the number of surface atoms and achieve more complete passivation of surface dangling bonds (*23*).

QDs may also be integrated in a matrix such as a conductive organic or inorganic host (such as polymers, chalcogenide glasses, oxides, or perovskites) (*12*). Early work in QD photovoltaics and photodetectors used semiconducting polymers, such as polythiophenes, to provide a charge-separating heterojunction (*28*, *29*). However, QD solids have progressed so rapidly in their charge carrier mobilities that the inclusion of a polymer phase typically leads to an undesired reduction in carrier mobility. In the area of light emission, the use of semiconducting polymers as a matrix material has had considerably more success (*30*). Infilling of QD solids through the atomic-layer deposition of oxides has been shown to increase the performance of QD electronics because the oxide matrix acts to passivate and stabilize QD surfaces (*31*, *32*). Recently, the organo-metal halide perovskite, a solution-processable semiconductor complementary to QDs, was successfully incorporated as a large band gap (type I) matrix (*33*) that produced a high degree of passivation of the incorporated QD phase. The perovskites, with their high mobilities, enabled efficient transport of photocharges to and capture across the hetero-interface with the QD inclusions.

QDs as tunable light absorbers and emitters

In bulk semiconductors, free carriers are generated by illumination with photons with energies above the band gap. The high dielectric constant of traditional bulk semiconductor leads to a small Coulomb binding energy of the electron and hole compared with thermal energy at room temperature. In contrast, quantum and dielectric confinement effects in semiconductor QDs give rise to strong optical absorption resonances associated with allowed transitions between discrete electronic states (Fig. 2A), producing electron-hole pairs with relatively large binding energies, thus creating single excitons (X) or multiple excitons [for example, biexcitons (BX)] at an amount depending on the QD absorption cross section at a given photon energy and the intensity of illumination (Fig. 3A, schemes for X and BX).

Electron-hole recombination in bulk crystals of direct band gap semiconductors typically occurs through radiative band-to-band transition. In direct band gap colloidal QDs, the band-to-band transitions have nearly monochromatic colors, with large oscillator strengths owing to the quantization of the electronic states (Fig. 3A). However, dangling bonds at the large-area surface create a high density of mid-gap trap states, introducing a competitive pathway to band-edge recombination. Ligand passivation can satisfy surface bonding and reduce the unintentional trap density and therefore the nonradiative, trap recombination. Another nonradiative route exists both in bulk and colloidal QDs: In the presence of high doping concentrations, recombination is typically dominated by the Auger process, involving the transfer of the electron-hole recombination energy to a neighboring third particle (electron or hole) and its ejection to a "hot" state. In QDs, the Auger process is more efficient with respect to the analogous process in the bulk because conservation of momentum is broken, strong spatial confinement of the carriers enhances multiple carrier Coulomb interactions (*34*), and proximal surface traps can accommodate ejected carriers (*35*). The Auger process leaves behind a charged QD that can interact with a subsequent excitation, forming a charged exciton (X^+) (an exemplary scheme for the Auger process is shown in Fig. 3A).

In addition to surface ligation, the QD surface may be engineered by synthesizing QDs in the

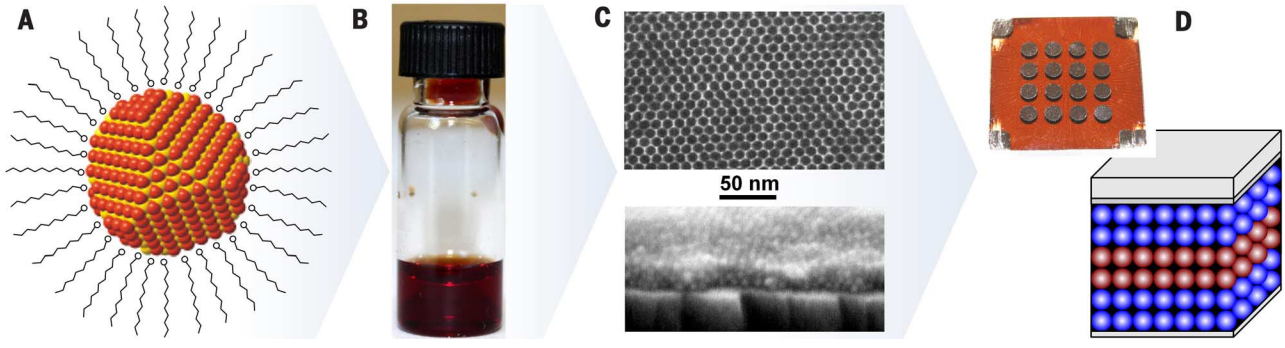

Fig. 1. Assembly of thin-film devices from colloidal QDs. (**A**) Schematic of an individual QD consisting of an inorganic semiconductor core surrounded by a layer of surface ligands. (**B**) The surface ligands stabilize the "QD ink," as seen by a photograph of a colloidal dispersion of QDs in a carrier solvent. (**C**) Colloidal dispersions of QDs can be cast or printed and form either glassy films with random packing of QDs (bottom) or long-range ordered QD superlattices (top), depending on the QD solvent evaporation rate and QD uniformity. (**D**) QD arrays are used as solution-deposited active components of electronic and optoelectronic devices such as transistors, light-emitting diodes, and solar cells (inset). Multiple QD layers can be stacked on top of each other by using chemically orthogonal solvents.

form of inorganic nano-heterostructures comprising a semiconductor core covered by another semiconductor as an epitaxial shell, forming type I and type II configurations. The band-offset in a type I core/shell heterostructure wraps the band edges of the core by that of the shell (Fig. 3B), confining the electron and hole into the core. In a type II or quasi–type II heterostructure, the core and shell band edges are staggered, permitting partial or complete extension of one carrier into the shell (Fig. 3B). This spatial separation of the electron and hole reduces exchange interactions and lowers radiative recombination rates. Thus, engineering the QD surface is a prerequisite for device design, in which type I core/shell QDs are beneficial for achieving high-photoluminescence quantum yields needed for efficient electroluminescence, whereas type II QDs provide charge separation beneficial for photovoltaic devices or photodetectors. Indeed, QDs with near unity luminescence efficiency and size-tunable emission colors are beginning to be exploited in today's technologies—for example, the size-dependent emission from core-shell InP/ZnS QDs is used to achieve vivid colors in Samsung televisions (*36*).

Multiple excitons (such as BX or triexciton) can be generated in individual QDs through the sequential absorption of multiple photons at high photoexcitation densities (*37*, *38*) or with multiple exciton generation (MEG) processes (Fig. 3A) (*39*–*42*) . MEG involves the excitation of a single electron-hole pair into a high-energy state (typically ≥2.7 times the band gap) to form the so-called "hot" exciton, followed by nonradiative relaxation (cooling) into band-edge states. The cooling process deposits sufficient energy to pump another electron-hole pair across the band gap. In other words, the primary "hot" exciton is converted into two (or more) excitons with the band-gap energy (Fig. 3A). MEG is a topic of major interest targeted toward multiplying the number of carriers in order to increase the efficiency of QD photovoltaic cells and photodetectors.

However, strongly interacting multiple excitons or multiple carriers occasionally lead to fluorescence intermittencies, also known as blinking. This phenomenon involves switching between bright luminescence, which is associated with the existence of neutral excitons (X or BX), and dark luminescence, which is associated with the formation of charged excitons (such as X^+) upon the occurrence of the Auger process (Fig. 3A). The blinking effect is a topic of a major concern because it limits the efficiency of optoelectronic devices. Therefore, nonblinking QDs are desired and have been synthesized in recent years by exploiting QD core/shell heterostructure design, making use of a giant shell (*43*), giant core (*44*), or alloying of the core-shell interface (*45*, *46*).

Connecting the dots

Arrays of solution-deposited colloidal QDs can be integrated in devices to modulate and transmit charge under bias and thereby produce and control an electrical current, convert an optical flux to electrical power, and use electrical current to generate light akin to bulk semiconductor devices. QD arrays provide added degrees of freedom for materials engineering because the electrical, optical, and thermal properties of a QD array are determined by the characteristics of and the communication between the individual QDs.

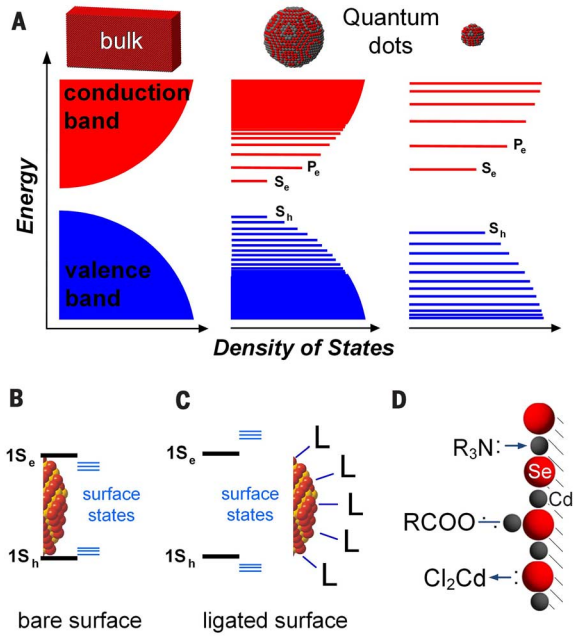

Fig. 2. The core and the surface of QDs. (**A**) Evolution of the electronic structure of inorganic semiconductors from bulk material to QDs of different size. (**B**) Broken chemical bonds at the QD surface introduce localized surface states inside the band gap. (**C**) Interaction of the QD surface atoms with ligand molecules alters the energy of the surface states, pushing them outside the band gap. (**D**) Diffrent types of chemical bonds between surface atoms and ligand molecules classified according to their chemical nature.

Electrical properties depend on the type, concentration, and mobility of charge carriers and the energy and density of states they occupy and through which they transport. In bulk semiconductor crystals, the carrier type and concentration are typically controlled by substitutional doping of electron donating or accepting impurity atoms in the lattice, and these carriers occupy and move with the mobility characteristic of the broad, high-density conduction and valence bands. In QD solids, the type and concentration of carriers may be similarly controlled by atoms in the QD core, but doping can be conveniently implemented by introducing atoms, ions, or ligands at the QD surface. These surface modifications may alter the observed carrier transport not only by acting as dopants, but also by shifting the QD energy levels and thereby the efficiency of carrier injection in devices (*18*, *47*). The efficiency of doping and the magnitude of the energy level shift depends on the type and oxidation state of the surface species and that of the QDs—and is an intriguing area only beginning to be explored. For example, nonstoichiometry created by the ligand type selected during synthesis (*26*), by means of surface atom stripping in solvents postsynthesis (*25*) or the physical or solution-based addition of atoms or ions (*48*–*50*), alter the polarity and magntiude of carrier transport (for example, arrays of PbSe QDs with excess Pb and excess Se show n- and p-type transport, respectively). Surface impurity atoms or ions and ligands can also serve as n- and p-dopants. For example, halide ligands have been shown to increase electron transport in PbS QD arrays (*51*). The additional carriers may occupy valence and conduction band states of the QDs or surface states, depending on the concentration of dopants in comparison with the mid-gap trap density.

In QD solids, the inorganic cores are separated by layers of surface ligands, creating relatively narrow, low-density conduction and valence band states (Fig. 3C). For charge to travel between the states of neighboring QDs, the carriers must transport through these interparticle layers with a tunneling rate $\Gamma \sim \exp\{-(2m^*\Delta E/\hbar^2)^{1/2}\Delta x\}$, where m^* is the electron effective mass, $\hbar$ is Planck's constant h divided by 2π, and ΔE and Δx are the height and width of the tunneling barrier defined by the ligands. The tunneling rate increases exponentially with decreasing separation between the QDs and is also very sensitive to the barrier height. The coupling between QDs is often expressed in terms of the coupling energy $\beta = \hbar\Gamma$, where $\hbar$ is Planck's constant and Γ is the tunneling rate described above. Here, we focus on the strong influence of the QD surface; however, charge transport in QD solids also depends on the size, size distribution, and organization of QDs in the arrays and has been reviewed elsewhere (*2*, *52*).

In a QD array, the effect of the intervening ligands that define energy barriers is multiplicative because of the large number of such barriers along the transport path of the charge carriers. In most cases, QD synthesis requires the use of long-chain organic ligands not suitable for electronic applications. Reducing Δx and ΔE by the proper design of the surface ligands increases the strength of electronic coupling between the QDs, and relatively small changes in ligand chemistry can dramatically alter the conductivity of the QD layer (*53*–*56*). The native ligands can be exchanged for shorter and conjugated organic molecules or compact inorganic compounds. The exponential increase in the mobility of charge carriers with

the shortening of organic ligand molecules is observed in films of PbSe QDs (*53*, *57*). The most mobile electron transport has been observed in arrays of QDs capped with inorganic ligands, represented by chalcogenidometallate (such as $Sn_2S_6^{4-}$, $In_2Se_4^{2-}$, and $CdTe_2^{2-}$) (*58*–*60*), halometallate ($PbCl_3^-$ and $InCl_4^-$) (*61*, *62*), chalcogenide (S^{2-}), halide (Cl^- and I^-), and pseudohalide (SCN^- and N_3^-) (*62*, *63*) ions. The combination of strong coupling by using compact ligand exchange and doping chemically, electrochemically (*64*), or electrostatically allows carriers to access higher-density and higher-mobility states. The recent introduction of high >10 $cm^2\ V^{-1}\ s^{-1}$ mobility QD solids (*48*, *60*, *65*, *66*) is enabling high-performance, solution-deposited QD electronics and fast carrier transport to outcompete multiple exciton quenching and carrier trapping and/or nonradiative Auger relaxation important for QD optoelectronics.

Inorganic shells in core/shell QDs can also contribute to the coupling strength among QDs. For type I heterostructures, the electronic states of the core material are substantially shielded within the QD and interact much less with their surroundings. This situation is favorable for high luminescence efficiency but not favorable for transport of electrons and holes between QDs. On the other hand, partial charge separation in type II heterostructures can enhance transport for one type of carrier (electrons or holes) while suppressing that of the other carrier (*65*).

Excitons can also be transferred between neighboring QDs (Fig. 3D). At interparticle separations of 0.5 to 10 nm, coupling through electromagnetic fields created by the transition dipoles of an excited QD (donor) and a ground-state QD (acceptor) lead to the radiationless transfer of excitons via Förster resonance energy transfer (FRET) (*67*). The efficiency of energy transfer is characterized by the Förster radius $R_o \propto \left(\frac{\phi_D}{n^4}\int_0^\infty F_D(\tilde{\nu})\varepsilon_A(\tilde{\nu})\frac{d\tilde{\nu}}{\tilde{\nu}^4}\right)^{1/6}$ in comparison with the physical center-to-center distance between donor and acceptor QDs, where ϕ_D is the donor QD emission quantum yield, $F_D(\tilde{\nu})$ the normalized spectrum of the excited donor QD emission, $\varepsilon_A(\tilde{\nu})$ is the molar extinction spectrum of the ground-state acceptor QD, and n is the refractive index of the QD array. FRET depends on the spectral overlap between QD donor emission and QD acceptor absorption, seen by the integrand, and therefore on the size and size distribution of the QDs and on the orientation of QDs in the solids. The surface chemistry of the QDs affects the efficiency of energy transfer through the emission quantum yield of the QDs, the refractive index of the array, and, as it increases, the center-to-center QD spacing, particularly as the ligand length or shell thickness become large compared with the QD diameter. At <0.5 nm interparticle distances, stronger exchange interactions lead to fast exciton diffusion.

FRET plays an important role in QD optoelectronic devices. In QD photovoltaics, energy transfer within the inhomogeneous distribution of QDs (*68*) leads to energy loss. In QD light-emitting devices, energy transfer in core-only QD arrays leads to undesirable self-quenching of the emission within the inhomogeneous distribution in QD states and to nonluminescent QDs, but energy transfer in core/shell QD arrays is believed to overcome poor charge injection, providing a route to QD excitation and to high-brightness QD devices (*69*).

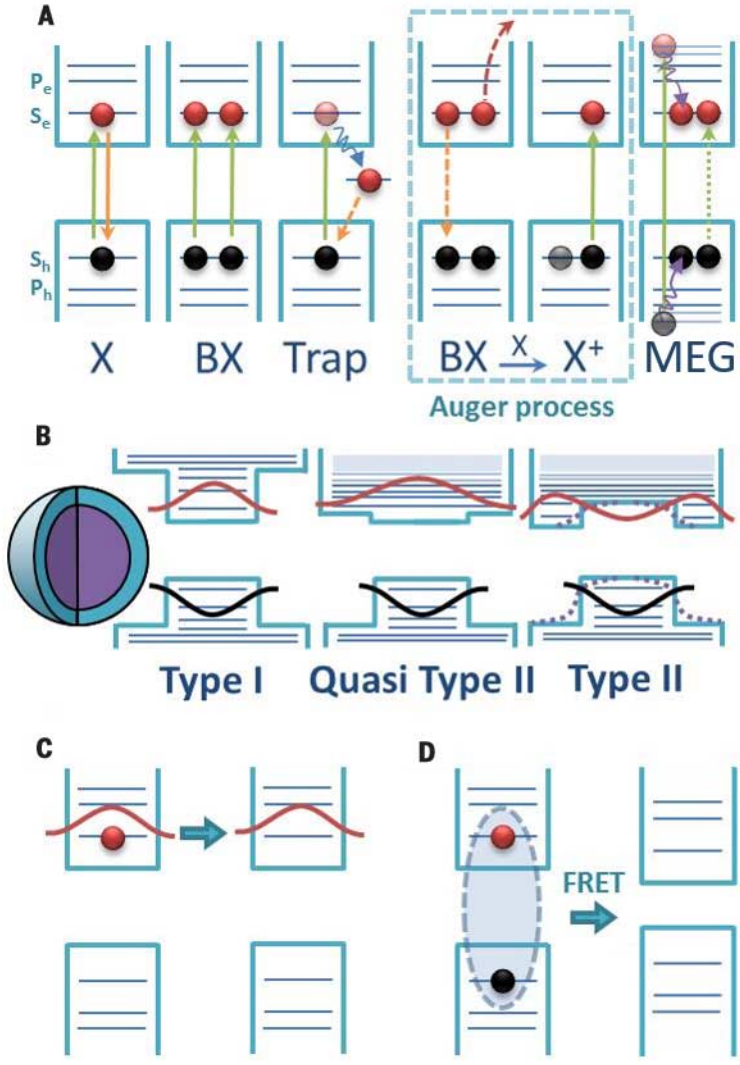

Fig. 3. Carrier dynamics and transport in QDs. (**A**) Schematic of absorption and emission processes in QDs. From left to right: band-edge absorption (green arrow) and emission (orange arrow) of a single exciton (X); sequential absorption of two photons in resonance with the band gap energy for the formation of a biexciton (BX); nonradiative decay of an electron (curled arrow) into a mid-gap trap state followed by trap-to-band recombination (dashed orange arrow); framed area: BX nonradiative Auger process, involving energy transfer from electron-hole recombination (dashed orange arrow) to a third carrier (such as an electron) and its ejection to a remote state (red dashed and curved arrow). The hole left behind (pale circle) becomes attached to a freshly formed exciton (X), creating a hole-hole-electron complex (trion, X^+); Multiple exciton generation (MEG) starts with the creation of an electron-hole pair with energy significantly above the band gap (pale circles), followed by nonradiative relaxation (cooling) into a band-edge state (curled arrows). The cooling energy enables the generation of additional electron-hole pair (or pairs) across the band-gap—the formation of multiple excitons. (**B**) Schematic of a core/shell heterostructure and (from left to right) type I, quasi-type II, and type-II core-to-shell band-edge alignments. Dashed lines in type II designate a smooth interface potential in the case of an alloyed boundary. (**C** and **D**) Schematics of (C) electron transfer between QDs via tunneling and (D) exciton transfer between QDs via FRET processes.

Understanding heat transport in QD arrays is another very important component of device engineering. For example, it has recently been shown that thermal runaway is the major obstacle to QD lasers (*70*). On the other hand, low thermal conductivity is naturally beneficial for thermoelectric applications. Unfortunately, little research effort has been devoted to this important subject. Several recent studies have revealed the key role of the QD surface in heat transport and to electron-phonon coupling strength (*71*). Reported values of the thermal conductivity of QD solids are in the range of 0.1 to 0.4 $Wm^{-1}\ K^{-1}$, which is about three orders of magnitude smaller

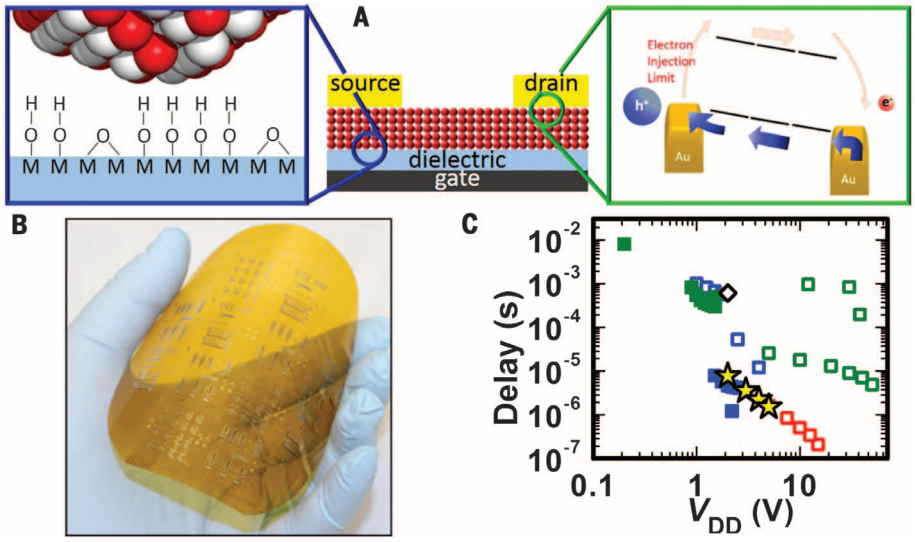

Fig. 4. QD electronics. (**A**) QD field-effect transistors highlighting the (left) semiconductor-gate dielectric interface, detailing the surface chemistry of commonly used oxides (*88*), and (right) metal-semiconductor interface, which introduces barriers to charge injection (*80*). (**B**) Large-area (40.64 cm^2) flexible QD electronic circuitry. (**C**) Comparison of the delay, a measure of the switching speed, as a function of supply voltage (V_{DD}) for flexible QD circuits (yellow stars) in comparison with rigid (solid symbols) and flexible (open symbols) solution-processable, semiconducting organic (green), carbon nanotube array (blue), sol-gel metal-oxide (red), and early QD channel layers (black) (*87*).

than the thermal conductivity of bulk Si (*72*). The analysis of QD solid thermal conductivity has used effective medium approximations (EMAs) that express the thermal conductivity of the composite in terms of the constituent volume fractions and thermal conductivities of the QDs and of the ligands. To achieve agreement with experiments, EMA must take into account thermal conductance across the interface between the QD core and the ligands, which depends on the overlap and coupling of the vibrational density of states for the QD core and the ligands (*72*, *73*). Available experimental observations and EMA modeling suggest that the ligand-ligand interface between neighboring QDs is critical to heat transfer and needs to be engineered to increase heat transport in QD solids.

Building devices from quantum dot solids

QD electronics

Colloidal QD solids have been incorporated as the semiconductor channel layer in thin-film field-effect transistors (FETs) (Fig. 4A). QD FETs provide a platform to probe carrier transport and as building blocks of low-cost, large-area, solution-processable, and flexible electronic technologies.

The FET uses the gate electrode to electrostatically shift the Fermi energy and modulate the majority carrier concentration and conductance of the QD thin-film channel spanning the source and drain electrodes and within the Debye length of the gate dielectric layer. The magnitude, voltage onset, and stability of the current and conductance modulation by the gate voltage are described by the metrics of mobility, current modulation, threshold (or turn-on) voltage, hysteresis, and subthreshold slope.

For electronic devices, the high carrier mobility (>10 $cm^2\ V^{-1}\ s^{-1}$) achieved through the combination of compact ligand exchange and surface passivation and doping (described above) is important to realizing high-performance circuitry. Synthetic methods that reduce the inhomogeneity in electronic structure of the QD building blocks and ligand exchange chemistries and processes that allow for compact ligand chemistries and yet the deposition of ordered QD assemblies promise increased mobilities, while retaining signatures of the quantum-confined building blocks (*52*). Alternatively, the compact chalcogenidometallate ligand chemistries have been shown to serve as a molecular "solder," allowing these QDs to provide a solution-processable precursor to bulk semiconductors with mobilities of >400 $cm^2\ V^{-1}\ s^{-1}$ (*60*). In addition to carrier mobility, FETs require a large gate-modulated current (I_{ON}/I_{OFF}) between the "ON" state and the "OFF" state. The current modulation is dominated by the gate-controlled change in carrier concentration. FETs constructed from QD solids with a high carrier concentration in the "OFF" state—such as that found in low-band-gap, high-intrinsic carrier concentration semiconductors (for example, IV-VI QD solids) or in highly doped QD solids—have undesirably limited current modulation. Current modulation >10^4 or even 10^5 are needed for analog and digital circuitry, and low pico-ampere "OFF" currents are required for display applications.

The construction of the FET introduces two interfaces with the semiconductor QD thin film solid that substantially affect device performance: One is with the gate dielectric layer, and the other is with the source and drain electrodes (Fig. 4A). The semiconductor–gate-dielectric interface typically introduces a density of trap states that tails from the conduction and valence band into the band gap and leads to an increase in carrier scattering and trapping. Selection of the gate dielectric material—such as replacing the SiO_2 layer with an Al_2O_3 or ZrO_2 layer (*66*, *74*, *75*) and/or tying up surface states with self-assembled monolayers—reduces the interface trap density from ~10^{13} cm^{-2} to 10^{12} cm^{-2}. The reduced interface trap density gives rise to an increase in FET mobility and subthreshold slope and a reduction in hysteresis. The higher dielectric constant of metal oxide gate dielectric materials allows for low-voltage operation. These strategies have similarly been used to improve the performance of one-dimensional (1D) nanowire and nanotube, 2D graphene, and organic semiconductor thin-film FETs (*76*–*79*).

The interface between metal source and drain electrodes and a semiconductor QD solid often introduces energetic barriers to charge injection (Fig. 4A) because metal electrodes create interface states that give rise to Fermi-level pinning. In weakly coupled QD solids, the high resistance of the channel layer dominates device performance. However, in the high-mobility, high-conductivity, strongly coupled QD solids of interest for electronics, complete or partial Fermi-level pinning may create more highly resistive electrical contacts, limiting charge injection and therefore controlling and ultimately determining FET polarity, mobility, and current level (*80*). As in the case of bulk semiconductor crystals, heavily doping the contact region by depositing a metal that also serves to dope the QD solid (*66*) provides a route to create Ohmic contacts.

The QD surface has been identified as a major culprit responsible for substantial device hysteresis; bias-stress instability, the degradation in device current under bias over time (*81*); and noise, the instantaneous fluctuations in the current (*82*, *83*). Infiltration and encapsulation of the FET QD thin-film solid with metal oxides grown by means of atomic layer deposition has been shown to reduce these instabilities (*32*, *83*). Continued advances and insight into the chemical species responsible for these instabilities will allow for a more targeted materials design to improve FET performance and therefore circuit operation.

To date, high-mobility colloidal QD FETs have been fabricated from II-VI, III-V, or IV-VI semiconductors. QD FETs from wider band gap II-VI and III-V semiconductors show high current modulation; however, only n-type FETs have been realized (*65*, *66*, *84*, *85*). In contrast, FETs from narrower bandgap IV-VI QDs show low current modulation yet can be doped n-type or p-type (*48*). Engineering the device interfaces (metal/semiconductor and semiconductor/gate dielectric) and metal oxide encapsulation has yielded low hysteresis and subthreshold swing and reduced bias stress and noise. These high-performance metrics of QD FETs are required to realize their operation, stability, and gain/speed in analog and digital circuits. These QD FETs were used as the

building blocks of integrated circuits, in which many transistors are connected on-chip (*86*, *87*). Multiple components of the FET device (semiconductor channel, metallic source and drain electrodes, and gate dielectric layer) can be constructed from colloidal nanoparticles, promising solution-phase circuit fabrication (*6*).

n-type II-VI QD FETs have been integrated to demonstrate all n-type circuits, referred to as NMOS (n-type metal oxide semiconductor) electronics, adopting the naming from conventional Si devices (Fig. 4B). These circuits include analog and digital topologies, namely inverters, negative-AND (NAND) and NOR logic gates, and ring oscillators for voltage amplification and switching (*87*). Methods to repair the QD surface after exposure to air and solvents have allowed QD circuit fabrication by using conventional clean room techniques (*88*). These techniques enable devices to be scaled down in dimension and scaled up in area so as to realize higher-bandwidth analog and higher-speed digital, large-area, QD integrated circuits. The low-temperature, solution processability of QD integrated circuits is compatible with fabrication of flexible circuitry, and their performance rivals that of other solution-processable semiconductors explored for flexible electronic devices. For example, solution-processable and flexible colloidal QD circuits show the highest switching speed at low voltages in comparison with solution-processable organic semiconductor (*89*, *90*), carbon nanotube array (*91*), and sol-gel metal oxide circuits (Fig. 4C) (*92*).

The demonstration of high-mobility QD-based semiconductors and further device scaling opens routes to continue to increase the speed of QD circuitry. However, NMOS circuitry is relatively limited in gain and speed and also has higher power dissipation than that of CMOS (complementary MOS) electronics constructed from a combination of n-type and p-type FETs. CMOS circuits—namely, two transistor inverters—have been fabricated from IV-VI QDs and show switching and higher gain (*80*, *93*), but these circuits are fundamentally limited by the narrow band gap of IV-VI QDs and therefore low current modulation. Design of high-mobility, high-current-modulation, and stable p-type QD FETs is needed to realize higher gain/higher speed CMOS QD circuitry. As an alternative, printable CMOS circuits can be constructed by combining n-type QDs with p-type organic electronic materials.

QD photoconductors

Absorption of photons may be used to control the conductivity of a QD solid, enabling application of these materials for light detection. The first generation of QD light detectors focused on photoconduction (*94*)—a light-sensing paradigm offering the advantage of signal amplification—and also leveraging rather than being limited by trap states, known in the photoconductor context as sensitizing centers (Fig. 5A). In the presence of such centers, photogeneration of an electron-hole pair is followed by capture of one carrier (we use electrons for illustration), whereas holes remain substantially free to travel. Symmetric contacting (Fig. 5A) can be used in this unipolar device. Photoholes are recirculated, and their photocurrent flows in proportion to their lifetime ratioed to their transit time. Photoconductive gain as large as 10^3 to 10^6 is possible as a result, and electron trapping—such as that enhanced by Auger-assisted ionization after multiple exciton generation (Fig. 2) (*95*)—favors the generation of additional signal.

The extended lifetimes of trapped photocarriers can be controlled via the QD surface chemistry, and early identification of surface oxides and sulfates was aided by studies that correlated QD surface composition with device response speed (*96*). Dark current is amplified via the same mechanism as that which provides photoconductive gain to photocharges, so within the classic resistive photoconductor, the ratio of light to dark current is increased only by minimizing dark free carrier density (*97*). The dark current has a lower bound defined by the intrinsic carrier density, and therefore photoconductors characteristically have undesirably high dark current density. Photodetectors based on QDs exploit tuning of the band-edge to a suitably chosen spectral cutoff energy, enabling dark current minimization for a given desired spectral response. Researchers have further overcome this limitation using gain-providing photo-field-effect transistors (*98*). The transistor introduces a threshold, so that turn-on occurs only after a certain photocarrier density (hence light level) is exceeded.

QD photodiodes and photovoltaics

QD photodiodes have been explored more recently in order to increase device speed and sensitivity, and QD photovoltaic devices (Fig. 5C) are of interest so as to harvest and convert solar energy and waste heat into electricity and, potentially, stored fuel (*99*). Compared with traditional silicon devices and organic semiconductors, QD solids are particularly suitable for efficiently capturing and detecting infrared photons, both in near- and mid-infrared regions (*100*, *101*).

Photodetectors and solar energy–harvesting devices should ideally achieve complete absorption above their band edge; as a result, they require thicknesses [or, when aided by photonic, plasmonic, or bulk heterojunction (*102*) techniques, an effective optical thicknesses] on the order of α^{-1}, where α is the absorption per unit length near the band edge. In QD solids, this is often assessed at the first excitonic peak, and the value of α^{-1} is ~ 500 to 1000 nm. Densifying the QD solid, first with high QD packing, is of interest, in order to increase the oscillator strength of absorbers, enhance the effective index of the medium, and maximize carrier capture. Superlattices achieve the highest packing, although the gap between random close packing (64%) and hexagonal/face-centered cubic close packing (74%) is not vast. Embedding dots in a high-index dielectric medium is of great interest, either via ligand design, the merging of shells, or epitaxial matrix growth (*33*).

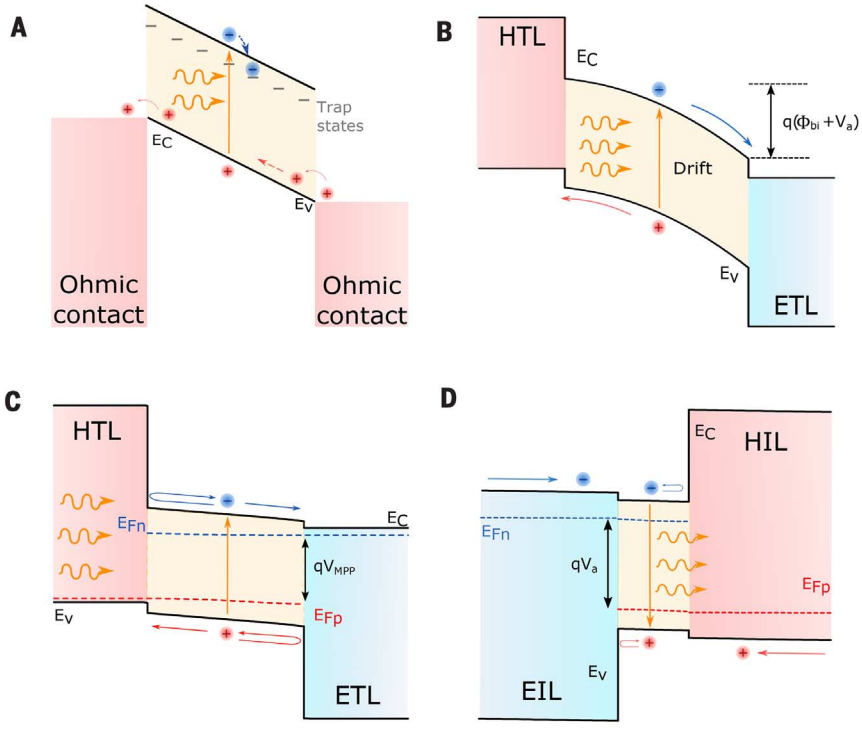

Fig. 5. QD optoelectronic devices. (**A**) Photoconductors, unipolar devices that include sensitizing centers to postpone recombination of one carrier class (electrons in the figure) while allowing the other carrier (holes in the figure) to flow. (**B**) Photodiodes that leverage the application of a voltage bias so as to achieve carrier separation and extraction. (**C**) Photovoltaics that must develop a photovoltage and rely on carrier diffusion, as well as on the use of selective contacts (an electron-accepting hole-blocker, and a hole-accepting electron blocker). (**D**) Light-emitting devices exploiting type-I heterojunctions.

Extracting photocarriers by using the built-in field in a photodiode (Fig. 5B, drift region) provides a ready path to achieving efficient photocurrent generation; when excited-state lifetimes are a typical ~100 ns, a built-in or applied potential on the order of 1 V can achieve a drift-based extraction time comparable with the excited lifetime when the lower of the electron or hole mobility exceeds 2×10^{-3} cm^2/Vs. Relative to the spectacular progress in QD FET mobilities, this is a modest requirement. QD photodetectors now reach bandwidths exceeding the megahertz frequencies (*100*); further progress into the gigahertz regime (relevant to centimeter-resolved time-of-flight sensing) will require mobilities exceeding 1 cm^2/Vs found in the strongly coupled QD solids.

In photodiodes, a reverse bias can be applied to supplement the built-in potential, and high internal quantum efficiency can be sustained even over thick active layers. A requirement of substantial applied potential does imply poor carrier diffusion in quasi-neutral material, and this may be a symptom of a high density of recombination-producing electronic trap states. In photodiodes, this does come with a disadvantage: States within the gap contribute to dark current generation, shrinking the effective band gap and enhancing thermal current generation. To produce photodiodes for highly sensitive detectors, it is desirable to satisfy the stringent conditions required of photovoltaic devices.

Solar cells must operate efficiently when transferring electric power to a load. This requires achieving high photocurrents while operating near the open-circuit (oc), hence flatband, condition (Fig. 5C). In the limit of approaching V_{oc}, at which point only recombination occurs, the separation of the quasi-Fermi levels in the active medium (which in turn provides an upper-bound on qV_{oc}) is desirably maximized. The requirements on efficient electroluminescent and photovoltaic devices are in fact one and the same: A maximal radiative efficiency is required of each (*103*).

From this perspective, QD solids have considerable room to improve. A first loss of V_{oc} comes from the Stokes shift that is inherent to individual QDs, which arises from the excitonic fine structure owing to the manifold of closely spaced optical transitions associated with the quasi-degenerate band edge states (*104*–*107*). Once QD films are formed, excitons and separated electron-hole pairs migrate among QDs and are funneled to the lowest-lying states in an inhomogeneously broadened ensemble. Light-emitting species present in QD solids—arising from QD aggregates or incorporated organic impurities—can potentially have a smaller photon emission energy and are capable in principle of additional undesired energy down-conversion (*108*).

Deep traps function as efficient recombination centers, impeding the generation of photocurrent in photovoltaic devices. It was recently found that present-day diffusion lengths in QD solids on the order of 100 nm can be accounted for by the one-part-per-10,000 density of deep trap recombination centers introduced by approximately one 5-nm, highly recombinative QD in a 100-nm cube of a QD solid (*109*). At present-day diffusion length values, increasing mobilities above 10^{-3} cm^2/Vs does not further benefit diffusion length because faster motion of carriers only leads to more efficient capture to traps (lifetime decreases as mobility increases). Carrier mobilities of 10^{-3} cm^2/Vs along with one-part-per-1000 deep trap state densities explain the best certified QD photovoltaic device power conversion efficiency (PCE) of 10.6% (*11*).

In order to approach the ultimate limit of solar cell performance by using QDs, the QD solid requires at least one of (i) minority carrier diffusion lengths exceeding the band-edge absorption length of ~ 1 μm; (ii) substantial densification of the QD solid to appreciably reduce the absorption length experienced by light near the band edge; or (iii) advanced photonic strategies to increase light absorption in an active medium having a single-pass absorbance. More modest progress along a few of these fronts would be sufficient to achieve substantial progress. The grand goal of a ~1 μm diffusion length should rely on part-per-10-million and lower deep trap state densities. This would entail QDs substantially free of bulk impurities, dislocations, and surface states, which lead to efficient recombination of excited photocarriers, and would rely on maintaining band gap integrity through avoidance of local aggregation and substantial loss of quantum confinement (*110*).

QDs-in-matrix (*33*, *60*) show promise, providing for the combination of increased dielectric constant for high absorption, epitaxial surface passivation for low-trap-state densities, and a smooth dielectric environment, which all work together in favor of increased minority carrier diffusion length and therefore solar cell efficiency.

QD electroluminescent devices

Light-emitting devices (Fig. 5D) based on QDs are of interest for displays in view of their spectrally narrow emission and size tunability, permitting a wide color gamut to be spanned. QDs also offer a qualitative benefit over organic and polymer materials because the emission of QD solids can extend into the near-infrared (NIR). This is of current interest for active illumination for gesture-recognition because the use of NIR light is invisible to the user and hence less intrusive than active visible-wavelength illumination. Many machine vision applications rely on active illumination of scenes by using structured light, ideally in the NIR.

External quantum efficiency (EQE) is a primary performance metric; it is the rate of emission into the final medium (such as free space) of photons, divided by the rate of injection of current expressed in electrons. Brightness translates into meeting a particular current density while keeping voltage efficiency high and ranges from milliamperes per square centimeter for displays and lighting to kiloamperes per square centimeter to enable lasing. An immediate first requirement for high EQE is high radiative efficiency within the QD active layer. Recent synthetic advances have produced excellent quantum yields (QYs) exceeding 97% in solution (*111*). Translating this into high luminescence efficiency in solid-state materials is an absolute requirement. The use of thick type I shells can keep the electron and hole wavefunction confined to the core, decreasing dependence on outer surface passivation; nevertheless, to achieve very high QYs a passivating ligand remains generally required. QDs in solids optimized for electroluminescent applications are therefore weakly interacting; exciton localization and efficient emission relative to nonradiative recombination outweigh the importance of carrier delocalization for transport. When high brightness is required, nonradiative processes such as the Auger process that arises under high-level injection conditions (Fig. 2A) must be forestalled—a topic of intense investigation in the QD synthesis community based on thick, graded, and type II shells (*112*–*114*).

The combination of the shells and ligands on the QD cores reduces carrier transport. Electroluminescent devices are fortunately not reliant on the very high electron and hole mobilities demanded of FETs. An effective QD electroluminescent device can be made on the basis of a single, light-emitting, QD monolayer and QD excitation via energy transfer of excitons or charge injection over only a few tens of nanometers in distance to form electron-hole pairs. Here, effective carrier injection and, crucially, effective blocking of carrier overflow are required. An electron-injection layer (Fig. 5D) is used to efficiently inject electrons into the light-emitting solid and block the egress of holes; the analogous qualities are desired of the hole injection layer. Translating quantitatively, very limited carrier mobilities of 10^{-6} cm^2/Vs (compatible with nanometer-thick shells and nanometer-long ligands) are adequate for tens of milliamperes per square centimeter of current to be injected into a QD-emitting monolayer at the modest price incurred in resistive overpotential (<0.1 V).

The result has been a rapid rate of progress in QD electroluminescent devices, reviewed elsewhere (*69*), leading to a recent 20.5% record EQE (*115*). Further frontiers for QD devices include increasing light extraction efficiencies via photonic and plasmonic structures, as has been achieved in organic LEDs (*116*), and exploiting QD matrix engineering for refractive index control so as to maximize light extraction. A further goal is to take QD electroluminescent devices beyond applications in displays and into the realm of lighting, projection, and lasing.

Summary and outlook

Unlike traditional bulk semiconductors whose electronic structure is locked in by their bonding at the atomic scale, semiconductor QDs introduce a new materials class from which to design solid-state electronic materials. Their properties may be rationally engineered in a one-at-a-time fashion by optimizing the largely independent degrees of freedom prized in individual QD building blocks and by engineering their surface chemistry to control the communication between

them. The chemical and physical properties of QD solids are being exploited in the low-cost, large-area, solution-based fabrication of QD electronic circuitry and optoelectronic light-emission, -sensing, and -harvesting devices and are now breaking through to find their introduction in technology.

The large-area surface of QDs and the many interconnections between QDs in solids present opportunities as well as a challenges. The dominant role of the surface and the wide range of materials chemistries that can be installed at the surface require continued advances in synthetic methods and their feedback with experimental probes and simulation to control the flow of charge, energy, and heat for specific device applications. In devices, the QD surface must be married with other materials, introducing interfaces that can govern device characteristics and performance. Engineering the interface between QD layers and other device components is in its infancy and promises to exploit new materials and methods in order to engineer the QD surface and optimize device performance.

REFERENCES AND NOTES

1. C. Murray, C. Kagan, M. G. Bawendi, Synthesis and characterization of monodisperse nanocrystals and close-packed nanocrystal assemblies. *Annu. Rev. Mater. Sci.* **30**, 545–610 (2000). doi: 10.1146/annurev.matsci.30.1.545
2. D. V. Talapin, J.-S. Lee, M. V. Kovalenko, E. V. Shevchenko, Prospects of colloidal nanocrystals for electronic and optoelectronic applications. *Chem. Rev.* **110**, 389–458 (2010). doi: 10.1021/cr900137k; pmid: 19958036
3. J. Yang, M. K. Choi, D.-H. Kim, T. Hyeon, Designed assembly and integration of colloidal nanocrystals for device applications. *Adv. Mater.* **28**, 1176–1207 (2016). doi: 10.1002/adma.201502851; pmid: 26707709
4. E. V. Shevchenko, D. V. Talapin, N. A. Kotov, S. O'Brien, C. B. Murray, Structural diversity in binary nanoparticle superlattices. *Nature* **439**, 55–59 (2006). doi: 10.1038/nature04414; pmid: 16397494
5. M. Cargnello *et al*., Substitutional doping in nanocrystal superlattices. *Nature* **524**, 450–453 (2015). doi: 10.1038/nature14872; pmid: 26310766
6. J.-H. Choi *et al*., Exploiting the colloidal nanocrystal library to construct electronic devices. *Science* **352**, 205–208 (2016). doi: 10.1126/science.aad0371; pmid: 27124455
7. L. E. Brus, Electron–electron and electron-hole interactions in small semiconductor crystallites: The size dependence of the lowest excited electronic state. *J. Chem. Phys.* **80**, 4403 (1984). doi: 10.1063/1.447218
8. A. I. Ekimov, A. L. Efros, A. A. Onushchenko, Quantum size effect in semiconductor microcrystals. *Solid State Commun.* **56**, 921–924 (1985). doi: 10.1016/S0038-1098(85)80025-9
9. L. Brus, Electronic wave functions in semiconductor clusters: Experiment and theory. *J. Phys. Chem.* **90**, 2555–2560 (1986). doi: 10.1021/j100403a003
10. A. H. Ip *et al*., Hybrid passivated colloidal quantum dot solids. *Nat. Nanotechnol.* **7**, 577–582 (2012). doi: 10.1038/nnano.2012.127; pmid: 22842552
11. X. Lan *et al*., Passivation using molecular halides increases quantum dot solar cell performance. *Adv. Mater.* **28**, 299–304 (2016). doi: 10.1002/adma.201503657; pmid: 26576685
12. M. A. Boles, D. Ling, T. Hyeon, D. V. Talapin, The surface science of nanocrystals. *Nat. Mater.* **15**, 141–153 (2016). doi: 10.1038/nmat4526; pmid: 26796733
13. A. Badia, L. Cuccia, L. Demers, F. Morin, R. B. Lennox, Structure and dynamics in alkanethiolate monolayers self-assembled on gold nanoparticles: A DSC, FT-IR, and deuterium NMR study. *J. Am. Chem. Soc.* **119**, 2682–2692 (1997). doi: 10.1021/ja963571t
14. A. Llordés, G. Garcia, J. Gazquez, D. J. Milliron, Tunable near-infrared and visible-light transmittance in nanocrystal-in-glass composites. *Nature* **500**, 323–326 (2013). doi: 10.1038/nature12398; pmid: 23955232
15. L. Protesescu *et al*., Atomistic description of thiostannate-capped CdSe nanocrystals: Retention of four-coordinate SnS4 motif and preservation of Cd-rich stoichiometry. *J. Am. Chem. Soc.* **137**, 1862–1874 (2015). doi: 10.1021/ja510862c; pmid: 25597625
16. D. Bozyigit, S. Volk, O. Yarema, V. Wood, Quantification of deep traps in nanocrystal solids, their electronic properties, and their influence on device behavior. *Nano Lett.* **13**, 5284–5288 (2013). doi: 10.1021/nl402803h; pmid: 24164600
17. Z. Hens, J. C. Martins, A Solution NMR Toolbox for characterizing the surface chemistry of colloidal nanocrystals. *Chem. Mater.* **25**, 1211–1221 (2013). doi: 10.1021/cm303361s
18. P. R. Brown *et al*., Energy level modification in lead sulfide quantum dot thin films through ligand exchange. *ACS Nano* **8**, 5863–5872 (2014). doi: 10.1021/nn500897c; pmid: 24824726
19. M. G. Panthani *et al*., Graphene-supported high-resolution TEM and STEM imaging of silicon nanocrystals and their capping ligands. *J. Phys. Chem. C* **116**, 22463–22468 (2012). doi: 10.1021/jp308545q
20. P. Guyot-Sionnest, B. Wehrenberg, D. Yu, Intraband relaxation in CdSe nanocrystals and the strong influence of the surface ligands. *J. Chem. Phys.* **123**, 074709 (2005). doi: 10.1063/1.2004818; pmid: 16229612
21. E. Lifshitz, Evidence in support of exciton to ligand vibrational coupling in colloidal quantum dots. *J. Phys. Chem. Lett.* **6**, 4336–4347 (2015).
22. P. Schapotschnikow, B. Hommersom, T. J. H. Vlugt, Adsorption and binding of ligands to CdSe nanocrystals. *J. Phys. Chem. C* **113**, 12690–12698 (2009). doi: 10.1021/jp903291d
23. D. Zherebetskyy *et al*., Hydroxylation of the surface of PbS nanocrystals passivated with oleic acid. *Science* **344**, 1380–1384 (2014). doi: 10.1126/science.1252727; pmid: 24876347
24. M. L. H. Green, A new approach to the formal classification of covalent compounds of the elements. *J. Organomet. Chem.* **500**, 127–148 (1995). doi: 10.1016/0022-328X(95)00508-N
25. N. C. Anderson, M. P. Hendricks, J. J. Choi, J. S. Owen, Ligand exchange and the stoichiometry of metal chalcogenide nanocrystals: Spectroscopic observation of facile metal-carboxylate displacement and binding. *J. Am. Chem. Soc.* **135**, 18536–18548 (2013). doi: 10.1021/ja4086758; pmid: 24199846
26. I. Moreels *et al*., Composition and size-dependent extinction coefficient of colloidal PbSe quantum dots. *Chem. Mater.* **19**, 6101–6106 (2007). doi: 10.1021/cm071410q
27. J. M. Luther, J. M. Pietryga, Stoichiometry control in quantum dots: A viable analog to impurity doping of bulk materials. *ACS Nano* **7**, 1845–1849 (2013). doi: 10.1021/nn401100n; pmid: 23527749
28. S. A. McDonald *et al*., Solution-processed PbS quantum dot infrared photodetectors and photovoltaics. *Nat. Mater.* **4**, 138–142 (2005). doi: 10.1038/nmat1299; pmid: 15640806
29. W. U. Huynh, J. J. Dittmer, A. P. Alivisatos, Hybrid nanorod-polymer solar cells. *Science* **295**, 2425–2427 (2002). doi: 10.1126/science.1069156; pmid: 11923531
30. G. J. Supran *et al*., QLEDs for displays and solid-state lighting. *MRS Bull.* **38**, 703–711 (2013). doi: 10.1557/mrs.2013.181
31. A. Pourret, P. Guyot-Sionnest, J. W. Elam, Atomic layer deposition of ZnO in quantum dot thin films. *Adv. Mater.* **21**, 232–235 (2009). doi: 10.1002/adma.200801313
32. Y. Liu *et al*., PbSe quantum dot field-effect transistors with air-stable electron mobilities above 7 cm2 V^{-1} s^{-1}. *Nano Lett.* **13**, 1578–1587 (2013). doi: 10.1021/nl304753n; pmid: 23452235
33. Z. Ning *et al*., Quantum-dot-in-perovskite solids. *Nature* **523**, 324–328 (2015). doi: 10.1038/nature14563; pmid: 26178963
34. D. Chepic *et al*., Auger ionization of semiconductor quantum drops in a glass matrix. *J. Lumin.* **47**, 113–127 (1990). doi: 10.1016/0022-2313(90)90007-X
35. J. Tang, R. A. Marcus, Mechanisms of fluorescence blinking in semiconductor nanocrystal quantum dots. *J. Chem. Phys.* **123**, 054704 (2005). doi: 10.1063/1.1993567; pmid: 16108682
36. E. Jang *et al*., White-light-emitting diodes with quantum dot color converters for display backlights. *Adv. Mater.* **22**, 3076–3080 (2010). doi: 10.1002/adma.201000525; pmid: 20517873
37. D. Oron, M. Kazes, I. Shweky, U. Banin, Multiexciton spectroscopy of semiconductor nanocrystals under quasi-continuous-wave optical pumping. *Phys. Rev. B* **74**, 115333 (2006). doi: 10.1103/PhysRevB.74.115333
38. R. Osovsky *et al*., Continuous-wave pumping of multiexciton bands in the photoluminescence spectrum of a single CdTe-CdSe core-shell colloidal quantum dot. *Phys. Rev. Lett.* **102**, 197401 (2009). doi: 10.1103/PhysRevLett.102.197401; pmid: 19518993
39. M. C. Beard *et al*., Multiple exciton generation in colloidal silicon nanocrystals. *Nano Lett.* **7**, 2506–2512 (2007). doi: 10.1021/nl071486l; pmid: 17645368
40. J. A. McGuire, J. Joo, J. M. Pietryga, R. D. Schaller, V. I. Klimov, New aspects of carrier multiplication in semiconductor nanocrystals. *Acc. Chem. Res.* **41**, 1810–1819 (2008). doi: 10.1021/ar800112v; pmid: 19006342
41. A. J. Nozik, Multiple exciton generation in semiconductor quantum dots. *Chem. Phys. Lett.* **457**, 3–11 (2008). doi: 10.1016/j.cplett.2008.03.094
42. A. Nozik, Quantum dot solar cells. *Phys. E Low-dimensional Syst. Nanostructures* **14**, 115–120 (2002). doi: 10.1016/S1386-9477(02)00374-0
43. Y. Chen *et al*., "Giant" multishell CdSe nanocrystal quantum dots with suppressed blinking. *J. Am. Chem. Soc.* **130**, 5026–5027 (2008). doi: 10.1021/ja711379k; pmid: 18355011
44. J. Tilchin *et al*., Quantum confinement regimes in CdTe nanocrystals probed by single dot spectroscopy: From strong confinement to the bulk limit. *ACS Nano* **9**, 7840–7845 (2015). doi: 10.1021/acsnano.5b02597; pmid: 26181051
45. M. Nasilowski, P. Spinicelli, G. Patriarche, B. Dubertret, Gradient CdSe/CdS quantum dots with room temperature biexciton unity quantum yield. *Nano Lett.* **15**, 3953–3958 (2015). doi: 10.1021/acs.nanolett.5b00838; pmid: 25990468
46. R. Vaxenburg, A. Rodina, E. Lifshitz, A. L Efros, Biexciton auger recombination in CdSe/CdS core/shell semiconductor nanocrystals. *Nano Lett.* **16**, 2503–2511 (2016). doi: 10.1021/acs.nanolett.6b00066; pmid: 26950398
47. A. M. Schimpf, K. E. Knowles, G. M. Carroll, D. R. Gamelin, Electronic doping and redox-potential tuning in colloidal semiconductor nanocrystals. *Acc. Chem. Res.* **48**, 1929–1937 (2015). doi: 10.1021/acs.accounts.5b00181; pmid: 26121552
48. S. J. Oh *et al*., Stoichiometric control of lead chalcogenide nanocrystal solids to enhance their electronic and optoelectronic device performance. *ACS Nano* **7**, 2413–2421 (2013). doi: 10.1021/nn3057356; pmid: 23368728
49. S. J. Oh *et al*., Designing high-performance PbS and PbSe nanocrystal electronic devices through stepwise, post-synthesis, colloidal atomic layer deposition. *Nano Lett.* **14**, 1559–1566 (2014). doi: 10.1021/nl404818z; pmid: 24499242
50. D. Kim, D.-H. Kim, J.-H. Lee, J. C. Grossman, Impact of stoichiometry on the electronic structure of PbS quantum dots. *Phys. Rev. Lett.* **110**, 196802 (2013). doi: 10.1103/PhysRevLett.110.196802; pmid: 23705733
51. Z. Ning *et al*., Air-stable n-type colloidal quantum dot solids. *Nat. Mater.* **13**, 822–828 (2014). doi: 10.1038/nmat4007; pmid: 24907929
52. C. R. Kagan, C. B. Murray, Charge transport in strongly coupled quantum dot solids. *Nat. Nanotechnol.* **10**, 1013–1026 (2015). doi: 10.1038/nnano.2015.247; pmid: 26551016
53. Y. Liu *et al*., Dependence of carrier mobility on nanocrystal size and ligand length in PbSe nanocrystal solids. *Nano Lett.* **10**, 1960–1969 (2010). doi: 10.1021/nl101284k; pmid: 20405957
54. D. V. Talapin, C. B. Murray, PbSe nanocrystal solids for n- and p-channel thin film field-effect transistors. *Science* **310**, 86–89 (2005). doi: 10.1126/science.1116703; pmid: 16210533
55. V. J. Porter, S. Geyer, J. E. Halpert, M. A. Kastner, M. G. Bawendi, Photoconduction in annealed and chemically treated CdSe/ZnS inorganic nanocrystal films. *J. Phys. Chem. C* **112**, 2308–2316 (2008). doi: 10.1021/jp710173q
56. N. C. Greenham, X. Peng, A. P. Alivisatos, Charge separation and transport in conjugated-polymer/semiconductor-nanocrystal composites studied by photoluminescence quenching and photoconductivity. *Phys. Rev. B Condens. Matter* **54**, 17628–17637 (1996). doi: 10.1103/PhysRevB.54.17628; pmid: 9985889
57. C. P. Collier, Reversible tuning of silver quantum dot monolayers through the metal-insulator transition. *Science* **277**, 1978–1981 (1997). doi: 10.1126/science.277.5334.1978
58. M. V. Kovalenko, M. I. Bodnarchuk, J. Zaumseil, J.-S. Lee, D. V. Talapin, Expanding the chemical versatility of colloidal

nanocrystals capped with molecular metal chalcogenide ligands. *J. Am. Chem. Soc.* **132**, 10085–10092 (2010). doi: 10.1021/ja1024832; pmid: 20593874
59. M. V. Kovalenko, M. Scheele, D. V. Talapin, Colloidal nanocrystals with molecular metal chalcogenide surface ligands. *Science* **324**, 1417–1420 (2009). doi: 10.1126/science.1170524; pmid: 19520953
60. D. S. Dolzhnikov *et al*., Composition-matched molecular "solders" for semiconductors. *Science* **347**, 425–428 (2015). doi: 10.1126/science.1260501; pmid: 25569110
61. D. N. Dirin *et al*., Lead halide perovskites and other metal halide complexes as inorganic capping ligands for colloidal nanocrystals. *J. Am. Chem. Soc.* **136**, 6550–6553 (2014). doi: 10.1021/ja5006288; pmid: 24746226
62. H. Zhang, J. Jang, W. Liu, D. V. Talapin, Colloidal nanocrystals with inorganic halide, pseudohalide, and halometallate ligands. *ACS Nano* **8**, 7359–7369 (2014). doi: 10.1021/nn502470v; pmid: 24988140
63. A. T. Fafarman *et al*., Thiocyanate-capped nanocrystal colloids: Vibrational reporter of surface chemistry and solution-based route to enhanced coupling in nanocrystal solids. *J. Am. Chem. Soc.* **133**, 15753–15761 (2011). doi: 10.1021/ja206303g; pmid: 21848336
64. M. Shim, P. Guyot-Sionnest, n-type colloidal semiconductor nanocrystals. *Nature* **407**, 981–983 (2000). doi: 10.1038/35039577; pmid: 11069172
65. J.-S. Lee, M. V. Kovalenko, J. Huang, D. S. Chung, D. V. Talapin, Band-like transport, high electron mobility and high photoconductivity in all-inorganic nanocrystal arrays. *Nat. Nanotechnol.* **6**, 348–352 (2011). doi: 10.1038/nnano.2011.46; pmid: 21516091
66. J. H. Choi *et al*., Bandlike transport in strongly coupled and doped quantum dot solids: A route to high-performance thin-film electronics. *Nano Lett.* **12**, 2631–2638 (2012). doi: 10.1021/nl301104z; pmid: 22509936
67. C. R. Kagan, C. B. Murray, M. Nirmal, M. G. Bawendi, Electronic energy transfer in CdSe quantum dot solids. *Phys. Rev. Lett.* **76**, 1517–1520 (1996). doi: 10.1103/PhysRevLett.76.1517; pmid: 10061743
68. C. R. Kagan, C. B. Murray, M. G. Bawendi, Long-range resonance transfer of electronic excitations in close-packed CdSe quantum-dot solids. *Phys. Rev. B Condens. Matter* **54**, 8633–8643 (1996). doi: 10.1103/PhysRevB.54.8633; pmid: 9984542
69. Y. Shirasaki, G. J. Supran, M. G. Bawendi, V. Bulović, Emergence of colloidal quantum-dot light-emitting technologies. *Nat. Photonics* **7**, 13–23 (2012). doi: 10.1038/nphoton.2012.328
70. M. M. Adachi *et al*., Microsecond-sustained lasing from colloidal quantum dot solids. *Nat. Commun.* **6**, 8694 (2015). doi: 10.1038/ncomms9694; pmid: 26493282
71. D. Bozyigit *et al*., Soft surfaces of nanomaterials enable strong phonon interactions. *Nature* **531**, 618–622 (2016). doi: 10.1038/nature16977; pmid: 26958836
72. W.-L. Ong, S. M. Rupich, D. V. Talapin, A. J. H. McGaughey, J. A. Malen, Surface chemistry mediates thermal transport in three-dimensional nanocrystal arrays. *Nat. Mater.* **12**, 410–415 (2013). doi: 10.1038/nmat3596; pmid: 23503009
73. M. Liu, Y. Ma, R. Y. Wang, Modifying thermal transport in colloidal nanocrystal solids with surface chemistry. *ACS Nano* **9**, 12079–12087 (2015). doi: 10.1021/acsnano.5b05085; pmid: 26553583
74. D. K. Kim, Y. Lai, T. R. Vemulkar, C. R. Kagan, Flexible, low-voltage, and low-hysteresis PbSe nanowire field-effect transistors. *ACS Nano* **5**, 10074–10083 (2011). doi: 10.1021/nn203948x; pmid: 22084980
75. D. S. Chung *et al*., Low voltage, hysteresis free, and high mobility transistors from all-inorganic colloidal nanocrystals. *Nano Lett.* **12**, 1813–1820 (2012). doi: 10.1021/nl203949n; pmid: 22385132
76. H. Klauk, U. Zschieschang, J. Pflaum, M. Halik, Ultralow-power organic complementary circuits. *Nature* **445**, 745–748 (2007). doi: 10.1038/nature05533; pmid: 17301788
77. W. Kim *et al*., Hysteresis caused by water molecules in carbon nanotube field-effect transistors. *Nano Lett.* **3**, 193–198 (2003). doi: 10.1021/nl0259232
78. C. M. Aguirre *et al*., The role of the oxygen/water redox couple in suppressing electron conduction in field-effect transistors. *Adv. Mater.* **21**, 3087–3091 (2009). doi: 10.1002/adma.200900550
79. J. Goldberger, D. J. Sirbuly, M. Law, P. Yang, ZnO nanowire transistors. *J. Phys. Chem. B* **109**, 9–14 (2005). doi: 10.1021/jp0452599; pmid: 16850973
80. S. J. Oh *et al*., Engineering charge injection and charge transport for high performance PbSe nanocrystal thin film devices and circuits. *Nano Lett.* **14**, 6210–6216 (2014). doi: 10.1021/nl502491d; pmid: 25298154
81. T. P. Osedach *et al*., Bias-stress effect in 1,2-ethanedithiol-treated PbS quantum dot field-effect transistors. *ACS Nano* **6**, 3121–3127 (2012). doi: 10.1021/nn3008788; pmid: 22480161
82. H. Liu, E. Lhuillier, P. Guyot-Sionnest, 1/f noise in semiconductor and metal nanocrystal solids. *J. Appl. Phys.* **115**, 154309 (2014). doi: 10.1063/1.4871682
83. Y. Lai *et al*., Low-frequency (1/f) noise in nanocrystal field-effect transistors. *ACS Nano* **8**, 9664–9672 (2014). doi: 10.1021/nn504303b; pmid: 25195975
84. W. Liu, J.-S. Lee, D. V. Talapin, III-V nanocrystals capped with molecular metal chalcogenide ligands: High electron mobility and ambipolar photoresponse. *J. Am. Chem. Soc.* **135**, 1349–1357 (2013). doi: 10.1021/ja308200f; pmid: 23267673
85. B. Sun, H. Sirringhaus, Solution-processed zinc oxide field-effect transistors based on self-assembly of colloidal nanorods. *Nano Lett.* **5**, 2408–2413 (2005). doi: 10.1021/nl051586w; pmid: 16351187
86. D. K. Kim, Y. Lai, B. T. Diroll, C. B. Murray, C. R. Kagan, Flexible and low-voltage integrated circuits constructed from high-performance nanocrystal transistors. *Nat. Commun.* **3**, 1216 (2012). doi: 10.1038/ncomms2218; pmid: 23169057
87. F. S. Stinner *et al*., Flexible, high-speed CdSe nanocrystal integrated circuits. *Nano Lett.* **15**, 7155–7160 (2015). doi: 10.1021/acs.nanolett.5b03363; pmid: 26407206
88. J.-H. Choi *et al*., In situ repair of high-performance, flexible nanocrystal electronics for large-area fabrication and operation in air. *ACS Nano* **7**, 8275–8283 (2013). doi: 10.1021/nn403752d; pmid: 23952742
89. H. Yan *et al*., Solution processed top-gate n-channel transistors and complementary circuits on plastics operating in ambient conditions. *Adv. Mater.* **20**, 3393–3398 (2008). doi: 10.1002/adma.200800629
90. L. Herlogsson, M. Cölle, S. Tierney, X. Crispin, M. Berggren, Low-voltage ring oscillators based on polyelectrolyte-gated polymer thin-film transistors. *Adv. Mater.* **22**, 72–76 (2010). doi: 10.1002/adma.200901850; pmid: 20217700
91. M. Ha *et al*., Aerosol jet printed, low voltage, electrolyte gated carbon nanotube ring oscillators with sub-5 μs stage delays. *Nano Lett.* **13**, 954–960 (2013). doi: 10.1021/nl3038773; pmid: 23394463
92. Y.-H. Kim *et al*., Flexible metal-oxide devices made by room-temperature photochemical activation of sol-gel films. *Nature* **489**, 128–132 (2012). doi: 10.1038/nature11434; pmid: 22955624
93. W. K. Koh, S. R. Saudari, A. T. Fafarman, C. R. Kagan, C. B. Murray, Thiocyanate-capped PbS nanocubes: Ambipolar transport enables quantum dot based circuits on a flexible substrate. *Nano Lett.* **11**, 4764–4767 (2011). doi: 10.1021/nl202578g; pmid: 22011060
94. G. Konstantatos *et al*., Ultrasensitive solution-cast quantum dot photodetectors. *Nature* **442**, 180–183 (2006). doi: 10.1038/nature04855; pmid: 16838017
95. V. Sukhovatkin, S. Hinds, L. Brzozowski, E. H. Sargent, Colloidal quantum-dot photodetectors exploiting multiexciton generation. *Science* **324**, 1542–1544 (2009). doi: 10.1126/science.1173812; pmid: 19541992
96. G. Konstantatos, L. Levina, A. Fischer, E. H. Sargent, Engineering the temporal response of photoconductive photodetectors via selective introduction of surface trap states. *Nano Lett.* **8**, 1446–1450 (2008). doi: 10.1021/nl080373e; pmid: 18399622
97. G. Konstantatos, J. Clifford, L. Levina, E. H. Sargent, Sensitive solution-processed visible-wavelength photodetectors. *Nat. Photonics* **1**, 531–534 (2007). doi: 10.1038/nphoton.2007.147
98. V. Adinolfi *et al*., Photojunction field-effect transistor based on a colloidal quantum dot absorber channel layer. *ACS Nano* **9**, 356–362 (2015). doi: 10.1021/nn5053537; pmid: 25558809
99. T. Abe *et al*., Molecular hydrogen evolution by organic p/n bilayer film of phthalocyanine/fullerene in the entire visible-light energy region. *J. Phys. Chem. C* **115**, 7701–7705 (2011). doi: 10.1021/jp1094992
100. J. P. Clifford *et al*., Fast, sensitive and spectrally tuneable colloidal-quantum-dot photodetectors. *Nat. Nanotechnol.* **4**, 40–44 (2009). doi: 10.1038/nnano.2008.313; pmid: 19119281
101. P. Guyot-Sionnest, J. A. Roberts, Background limited mid-infrared photodetection with photovoltaic HgTe colloidal quantum dots. *Appl. Phys. Lett.* **107**, 253104 (2015). doi: 10.1063/1.4938135
102. Z. Ren *et al*., Amorphous TiO_2 buffer layer boosts efficiency of quantum dot sensitized solar cells to over 9%. *Chem. Mater.* **27**, 8398–8405 (2015). doi: 10.1021/acs.chemmater.5b03864
103. O. D. Miller, E. Yablonovitch, S. R. Kurtz, Strong internal and external luminescence as solar cells approach the Shockley–Queisser limit. *IEEE J. Photovoltaics* **2**, 303–311 (2012). doi: 10.1109/JPHOTOV.2012.2198434
104. W. Yoon *et al*., Enhanced open-circuit voltage of PbS nanocrystal quantum dot solar cells. *Sci. Rep.* **3**, 2225 (2013). doi: 10.1038/srep02225; pmid: 23868514
105. C. Li *et al*., Large Stokes shift and high efficiency luminescent solar concentrator incorporated with CuInS2/ZnS quantum dots. *Sci. Rep.* **5**, 17777 (2015). doi: 10.1038/srep17777; pmid: 26642815
106. W. Ma, J. M. Luther, H. Zheng, Y. Wu, A. P. Alivisatos, Photovoltaic devices employing ternary PbS_xSe_{1-x} nanocrystals. *Nano Lett.* **9**, 1699–1703 (2009). doi: 10.1021/nl900388a; pmid: 19351196
107. J. M. An, A. Franceschetti, A. Zunger, The excitonic exchange splitting and radiative lifetime in PbSe quantum dots. *Nano Lett.* **7**, 2129–2135 (2007). doi: 10.1021/nl071219f
108. G. H. Carey, L. Levina, R. Comin, O. Voznyy, E. H. Sargent, Record charge carrier diffusion length in colloidal quantum dot solids via mutual dot-to-dot surface passivation. *Adv. Mater.* **27**, 3325–3330 (2015). doi: 10.1002/adma.201405782; pmid: 25899173
109. D. Zhitomirsky *et al*., Engineering colloidal quantum dot solids within and beyond the mobility-invariant regime. *Nat. Commun.* **5**, 3803 (2014). doi: 10.1038/ncomms4803; pmid: 24801435
110. A. H. Ip *et al*., Infrared colloidal quantum dot photovoltaics via coupling enhancement and agglomeration suppression. *ACS Nano* **9**, 8833–8842 (2015). doi: 10.1021/acsnano.5b02164; pmid: 26266671
111. O. Chen *et al*., Compact high-quality CdSe-CdS core-shell nanocrystals with narrow emission linewidths and suppressed blinking. *Nat. Mater.* **12**, 445–451 (2013). doi: 10.1038/nmat3539; pmid: 23377294
112. J. Lim *et al*., Influence of shell thickness on the performance of light-emitting devices based on $CdSe/Zn_{1-X}\ Cd_X\ S$ core/shell heterostructured quantum dots. *Adv. Mater.* **26**, 8034–8040 (2014). doi: 10.1002/adma.201403620; pmid: 25381683
113. B. N. Pal *et al*., 'Giant' CdSe/CdS core/shell nanocrystal quantum dots as efficient electroluminescent materials: Strong influence of shell thickness on light-emitting diode performance. *Nano Lett.* **12**, 331–336 (2012). doi: 10.1021/nl203620f; pmid: 22148981
114. S. A. Ivanov *et al*., Type-II core/shell CdS/ZnSe nanocrystals: Synthesis, electronic structures, and spectroscopic properties. *J. Am. Chem. Soc.* **129**, 11708–11719 (2007). doi: 10.1021/ja068351m; pmid: 17727285
115. X. Dai *et al*., Solution-processed, high-performance light-emitting diodes based on quantum dots. *Nature* **515**, 96–99 (2014). doi: 10.1038/nature13829; pmid: 25363773
116. S. Reineke *et al*., White organic light-emitting diodes with fluorescent tube efficiency. *Nature* **459**, 234–238 (2009). doi: 10.1038/nature08003; pmid: 19444212

ACKNOWLEDGMENTS

C.R.K. gratefully acknowledges the U.S. Department of Energy, Office of Basic Energy Sciences, Division of Materials Science and Engineering, under award DE-SC0002158 for support. E.L. thanks the Israel Council for High Education–Focal Area Technology (grant 872967), the Volkswagen Stiftung (grants 88116 and ZN2916), the Israel Science Foundation (grants 914/15 and 1508/14), and the Horizon2020 PHONSI project for their support. E.H.S. acknowledges award (KUS-11-009-21) from the King Abdullah University of Science and Technology (KAUST). D.V.T. acknowledges support by the U.S. Department of Defense (DOD) Office of Naval Research grant N00014-13-1-0490. C.R.K., E.H.S., and D.V.T. hold and have applied for several patents related to QD assemblies in devices. E.H.S. has a financial interest in and serves as Chief Technology Officer and director of InVisage Technologies.

10.1126/science.aac5523

Building devices from colloidal quantum dots
Cherie R. Kagan, Efrat Lifshitz, Edward H. Sargent and Dmitri V. Talapin (August 25, 2016)
Science **353** (6302), . [doi: 10.1126/science.aac5523]

Editor's Summary

From quantum dot to quantum dot

A wide range of materials can now be synthesized into semiconducting quantum dots. Because these materials grow from solutions, there is scope to combine quantum dots into devices by using simple, low-cost manufacturing processes. Kagan *et al.* review recent progress in tailoring and combining quantum dots to build electronic and optoelectronic devices. Because it is possible to tune the size, shape, and connectivity of each of the quantum dots, there is potential for fabricating electronic materials with properties that are not available in traditional bulk semiconductors.

Science, this issue p. 885

Science (print ISSN 0036-8075; online ISSN 1095-9203) is published weekly, except the last week in December, by the American Association for the Advancement of Science, 1200 New York Avenue NW, Washington, DC 20005.